Electronic structure of the strongly hybridized ferromagnet $CeFe_2$

T. Konishi,* K. Morikawa, K. Kobayashi, T. Mizokawa, and A. Fujimori
Department of Physics and Department of Complexity Science and Engineering, University of Tokyo, Bunkyo-ku, Tokyo 113-0033, Japan

K. Mamiya
Hiroshima Synchrotron Radiation Research Center, Hiroshima University, Higashi-Hiroshima 739-8526, Japan

F. Iga
Department of Quantum Matter, ADSM, Hiroshima University, Higashi-Hiroshima 739-8526, Japan

H. Kawanaka
Electrotechnical Laboratory, Tsukuba, Ibaraki 305-8568, Japan

Y. Nishihara
Faculty of Science, Ibaraki University, Mito, Ibaraki 310-8512, Japan

A. Delin
Fritz-Haber-Institut der Max-Planck-Gesellschaft, Faradayweg 4-6, D-14195 Berlin-Dahlem, Germany

O. Eriksson
Department of Physics, Uppsala University, P. O. Box 530, S-75121 Uppsala, Sweden
(Received 22 June 2000)

We report on results from high-energy spectroscopic measurements on $CeFe_2$, a system of particular interest due to its anomalous ferromagnetism with an unusually low Curie temperature and small magnetization compared to the other rare-earth iron Laves phase compounds. Our experimental results, obtained using core-level and valence-band photoemission, inverse photoemission and soft x-ray absorption techniques, indicate very strong hybridization of the Ce $4f$ states with the delocalized band states, mainly the Fe $3d$ states. In the interpretation and analysis of our measured spectra, we have made use of two different theoretical approaches: The first one is based on the Anderson impurity model, with surface contributions explicitly taken into account. The second method consists of band-structure calculations for bulk $CeFe_2$. The analysis based on the Anderson impurity model gives calculated spectra in good agreement with the whole range of measured spectra, and reveals that the Ce $4f$-Fe $3d$ hybridization is considerably reduced at the surface, resulting in even stronger hybridization in the bulk than previously thought. The band-structure calculations are *ab initio* full-potential linear muffin-tin orbital calculations within the local-spin-density approximation of the density functional. The Ce $4f$ electrons were treated as itinerant band electrons. Interestingly, the Ce $4f$ partial density of states obtained from the band-structure calculations also agree well with the experimental spectra concerning both the $4f$ peak position and the $4f$ bandwidth, if the surface effects are properly taken into account. In addition, results, notably the partial spin magnetic moments, from the band-structure calculations are discussed in some detail and compared to experimental findings and earlier calculations.

I. INTRODUCTION

The $4f$ states of rare-earth elements in solids usually retain free-ionic properties with a well-defined integer occupation number. However, there are also rare-earth compounds where the hybridization of the $4f$ states with extended band states is important, in which case they may exhibit properties usually only found in actinide systems. In such systems, many unusual phenomena are typically observed, like, for instance, anomalously low saturation magnetization and Curie temperature T_C (e.g., $CeFe_2$), intermediate valence (e.g, SmS), heavy fermion behavior (e.g., YbBiPt), or non-Fermi-liquid behavior (e.g., $CeCu_{6-x}Au_x$). Even more surprisingly, simultaneous magnetic ordering and superconductivity has been observed (e.g., $CeCu_2Si_2$). The superconductivity is unconventional, i.e., the order parameter suggests a *d*-wave superconducting state, as opposed to the conventional *s*-wave state. Finding a proper theoretical description of the $4f$ states in these compounds remains one of the major problems in condensed-matter physics.[1]

As for the photoemission spectroscopy (PES) studies of Ce compounds, it is widely believed that the spectra are well described by the single-impurity Anderson model (SIAM).[2] Recently, however, it has been argued that systems, in which the Ce $4f$ states hybridize strongly with the other valence electrons, calculations based on density-functional theory (DFT) may give an equally good, or even better description of the photoemission spectra than the SIAM analysis, provided that surface effects are properly taken into account in the analysis.[3] However, one should bear in mind that calcu-

lations based on DFT are not strictly applicable for excited-state properties, instead the ground-state properties, such as the magnetic moments of the ground state, which are typically the focus of these calculations. Nevertheless, the electronic structure given from such calculations are often compared with photoemission data and good agreement between experiment and calculations is frequently observed. In the limit of complete screening of the excited state, one would expect ground-state density-functional calculations to be able to describe the spectra well.

$CeFe_2$ is thought to belong to a class of strongly hybridized systems. This compound shows ferromagnetism below $T_C = 230$ K with a saturation magnetization of $2.30\mu_B$/f.u. Above T_C, the magnetic susceptibility follows the Curie-Weiss law with an effective moment of $7.4\mu_B$/f.u.[4] If one compares $CeFe_2$ with the other RFe_2 compounds (R: rare-earth elements), a number of anomalies in its physical properties can be observed. The lattice constant is much smaller than an interpolation using the lattice constants of the other RFe_2 systems would suggest. Its Curie temperature is anomalously low: the other RFe_2 compounds have Curie temperatures ranging from 596 to 796 K.[5] The saturation magnetization is unusually low compared to the other RFe_2 compounds (2.93 and $2.90\mu_B$/f.u. for $LuFe_2$ and YFe_2, respectively[5]). Moreover, even if only a small fraction of the Fe atoms are substituted for Al, the ferromagnetic ordering is destroyed, and the system becomes antiferromagnetic.[6] In fact, even in pure $CeFe_2$, recent neutron-scattering experiments have revealed strong competition between the ferromagnetic ground state and an antiferromagnetic ground state.[7] Together, these facts suggest that the Ce $4f$ states in $CeFe_2$ hybridize strongly with the other valence electrons, notably the Fe $3d$ valence states. This hypothesis is further supported by the x-ray-absorption (XAS) experiments by Croft *et al.*[8]

In this paper, we present high-energy spectroscopic results on $CeFe_2$ including core-level x-ray photoemission (XPS), XAS, Ce $3d$-$4f$ and $4d$-$4f$ resonant PES, bremsstrahlung isochromat (BIS), and high-resolution ultraviolet photoemission spectroscopy (UPS) in order to elucidate the electronic structure of this system. In the case of Ce compounds with strongly hybridized $4f$ states, it has been pointed out that surface effects are extremely important in the interpretation of the spectra.[9–11] Therefore we have attempted to differentiate the electronic structure of bulk and that of surface for $CeFe_2$ in the analysis of the spectra. As will be further elaborated on in Sec. III C of this paper, electronic-structure calculations with the Ce $4f$ states treated as valence states give a good description of the magnetism in $CeFe_2$.[12,13] It is of course highly interesting to assess the applicability of the same theory in describing also the photoemission spectra of $CeFe_2$, even though as noted these calculations are not strictly applicable for excited-state properties. Very recently, Sekiyama *et al.*[14] reported a high-resolution $3d$-$4f$ resonant photoemission study of the strongly hybridized system $CeRu_2$ and found that the Ce $4f$ spectra can be explained by band theory. In the following, we first attempt to describe the spectra in the framework of the SIAM and obtain a set of SIAM parameters. In the analysis, surface effects on the spectra are explicitly taken into account. Next, the bulk component of the valence-band spectra is compared with the density of states calculated using density-functional theory. All DFT results presented here have been calculated within the local spin-density approximation (LSDA). The use of more recently developed generalized gradient functionals would not, however, alter any of our conclusions.

II. METHODS

A. Experiment

Polycrystalline samples of $CeFe_2$ were prepared by arc melting the pure constituent materials. Subsequently, the samples were annealed at 750 °C for a week to obtain single phase samples. Magnetization measurements yielded the same T_C as in the literature. The XPS spectra were taken with Mg $K\alpha$ radiation ($h\nu = 1253.6$ eV) using a double-pass cylindrical-mirror analyzer, and the BIS spectra were obtained using a Pierce-type electron-gun and a quartz crystal monochromator which was set at $h\nu = 1486.6$ eV. The Ce $4d$-$4f$ resonant PES measurements were done at beam-line BL-2 of SOR-RING, Institute for Solid State Physics, University of Tokyo. The Ce $3d$-$4f$ resonant PES and Ce $3d$ XAS data were taken at beam-line BL-2B of Photon Factory, High Energy Accelerator Research Organization. Photoelectrons were collected using a double-pass cylindrical-mirror analyzer in the resonant PES measurements. The XAS spectra were obtained by measuring the total electron yield using an electron multiplier placed near the sample. All measurements were done in the range 50–80 K, i.e., below the Curie temperature. In the case of the Ce $4d$-$4f$ resonant PES, additional measurements at room temperature, i.e., above the Curie temperature, were performed. The total energy resolution was ~1.0 eV for XPS and BIS, ~0.5 eV for Ce $4d$-$4f$ resonant PES, ~0.5 eV for XAS, and ~1.0 eV for Ce $3d$-$4f$ resonant PES. The high-resolution UPS measurements were done around 17 K using a hemispherical analyzer and the He I ($h\nu = 21.2$ eV) and He II ($h\nu = 40.8$ eV) resonance lines. The energy resolution was ~25 meV for both photon energies. The binding energies were calibrated using Au evaporated on the samples. For XAS and Ce $3d$-$4f$ resonant PES, the photon energies were calibrated using the Cu $2p$ edge of Cu metal and the Co $2p$ peak of $LaCoO_3$. Clean surfaces were obtained by scraping the sample repeatedly, while maintaining the sample under ultrahigh vacuum, with a diamond file prior to each measurement. Cleanliness of the surfaces was checked by the absence of O $1s$ and C $1s$ XPS signals from contaminants in the case of the XPS, XAS, BIS, and Ce $3d$-$4f$ resonant PES measurements. In the case of the high-resolution UPS and Ce $4d$-$4f$ resonant PES measurements, cleanliness was checked by the absence of a O $2p$ feature which appears around 6 eV below the Fermi level (E_F).

B. Single-impurity Anderson model

The SIAM calculations were made based on the variational $1/N_f$-expansion method developed by Gunnarsson and Schönhammer.[15] Here, we performed the calculations to the lowest order in $1/N_f$, where N_f is the degeneracy of the Ce $4f$ level and was taken to be 14. The f^2 configuration was also included in the calculation. The energy dependence of

the hybridization matrix elements was taken from the off-resonant spectra, which approximately represent the Fe $3d$ partial density of states. The configuration dependence of the hybridization strength was also taken into account, and was chosen to be the same as that obtained for α-Ce by Gunnarsson and Jepsen.[16] In the calculations, we divided the band continuum into discrete levels following Kotani *et al.*[17] We further assumed that each spectrum was a superposition of two components which represent bulk and surface spectra. The weight of each component was treated as fitting parameters within a range consistent with the universal curve for the mean free path of photoelectrons.[18]

C. Band-structure calculation

In the band-structure calculations presented here, we have used the full-potential linear muffin-tin orbital method (FP-LMTO).[19] In this method, the Kohn-Sham equations[20] are solved for a general potential without any shape approximation. The local (spin) density approximation (LSDA) in the Hedin-Lundqvist parametrization[21] was used for the density functional.

In the FP-LMTO method, space is divided into nonoverlapping spheres, so-called muffin-tin spheres,[22] surrounding each atomic site, and an interstitial region. The basis functions used are energy-independent Bloch functions, whose construction is different in the spheres and in the interstitial.

A basis function in the interstitial is defined by the Bloch function of solutions to the spherical Helmholtz equation with nonzero kinetic energy κ^2, or a linear combination of such solutions for different kinetic energies. The Fourier representation of this basis function is taken from the Fourier series of a function matching the basis in the interstitial region but not inside the spheres, a so-called pseudowave function, whose exact shape inside the muffin-tin sphere is of no importance for the final solution as long as it is continuous and differentiable at the sphere boundary and matches the true basis function in the interstitial.

Inside the spheres, where the charge density varies rapidly, the basis functions are Bloch functions of numerical radial functions times spherical harmonics. The radial part of a basis function is constructed from the numerical solutions $\phi_L(E_\nu,r)$ of the radial Schrödinger equation in a spherical potential at the fixed energy E_ν, and their energy derivatives $\dot{\phi}_L(E_\nu,r)$. Here, the index L stands for a collection of quantum numbers: the principal quantum number n, the orbital quantum number l, the magnetic quantum number m, and the kinetic energy κ^2.

The treatment of the entire basis set within one single energy panel allows all states, including the semicore states, to hybridize fully with each other. Our method is linear, i.e., the basis functions are constructed by expanding around fixed energies E_ν. The expressions for the crystal wave functions in the muffin-tin spheres are matched to the interstitial crystal wave function at the sphere boundaries so that the total crystal wave function becomes continuous and differentiable in all space. In the present calculation, the expansion in spherical harmonics was taken up to $l=6$. For Ce, the $6s$, $5p$, $6p$, $5d$, and $4f$ orbitals were included in the basis set, with $5p$ as semicore. For Fe, we included the $4s$, $4p$, and $3d$ orbitals, i.e., no semicore state was used for Fe. Four

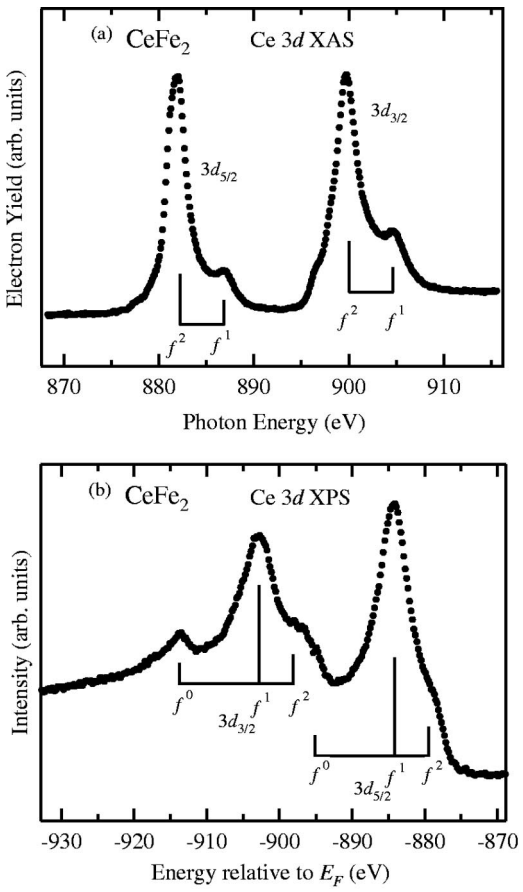

FIG. 1. Core-level spectra of $CeFe_2$. (a) Ce $3d$ core-level XAS spectra. (b) Ce $3d$ XPS spectra taken at $h\nu=1253.6$ eV.

κ^2 values were used in the calculation: -0.6 and -0.1 Ry for the valence states, and -1.5 and -1.0 Ry for the semicore Ce $5p$ states, all with respect to the muffin-tin zero.

Reciprocal space was sampled with what would correspond to 1331 **k** points in the full Brillouin zone (BZ) using special **k**-point sampling methods.[23] The nonoverlapping muffin-tin spheres were chosen as 21 and 17% of the unit-cell lattice constant for Ce and Fe, respectively. With this choice, 36% or the unit-cell volume is in the interstitial region and the closest muffin-tin spheres are 3% from touching.

The experimental lattice constant was used in the calculations. Furthermore, the calculations were spin polarized but the spin-orbit interaction was not included. This latter approximation will be commented on further in conjunction with presenting and discussing the results from the band-structure calculation.

III. RESULTS

A. Experiment

Figure 1 shows the Ce $3d$ core-level XPS and XAS spectra. The XPS line shape is a typical one for a strongly hybridized Ce compound, consisting of three peaks which correspond to the $3d^94f^0$, $3d^94f^1$, and $3d^94f^2$ final states in each of the $j=3/2$ and $5/2$ spin-orbit components.[24,25] In the XAS spectrum, the main peaks are due to the $3d^94f^2$ final-

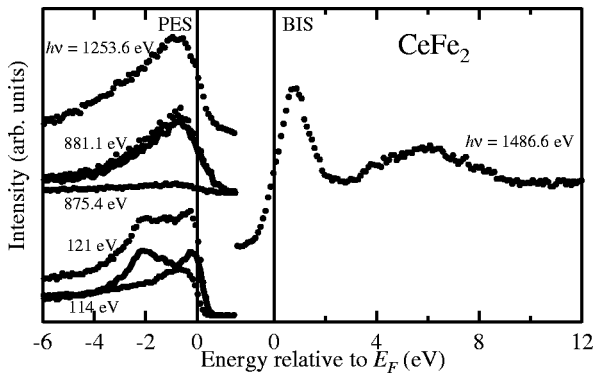

FIG. 2. Valence-band PES and BIS spectra of $CeFe_2$. $h\nu = 121$ and 114 eV (881 and 875 eV) correspond to Ce $4d$-$4f$ ($3d$-$4f$) on and off resonance, respectively. Solid curves show the difference spectra, which represent the Ce $4f$ component.

state multiplet and the satellite structures ~ 5 eV above the main peaks are due to the $3d^9 4f^1$ final states. The rather distinct $4f^0$ peaks in the XPS spectrum and the $4f^1$ structures in the XAS spectra, together with the obscured $3d^9 4f^2$ final-state multiplet structures of the main XAS peaks, indicate strong hybridization of the $4f$ states with the valence band in this system. The XPS spectrum reflects the surface electronic structure because of the rather low kinetic energies of photoelectrons from the Ce $3d$ core level. A detailed analysis of this is given below.

The results of valence-band PES and BIS are shown in Fig. 2. The on- and off-resonance occurs, respectively, at $h\nu = 121$ and 114 eV in the Ce $4d$-$4f$ resonant PES and at $h\nu = 881.1$ and 875.4 eV in the Ce $3d$-$4f$ resonant PES. Identical spectra in the present resolution have been obtained for Ce $4d$-$4f$ resonant PES at room temperature, which is above T_C (not shown). We have obtained the Ce $4f$ spectra by subtracting the off-resonance spectra from the on-resonance spectra as shown by solid curves in Fig. 2. As seen from this figure, there is a large difference between the Ce $4f$ spectra obtained from the Ce $4d$-$4f$ and Ce $3d$-$4f$ resonant PES. While the former has a double-peak structure in the vicinity of -2 eV and near E_F, the latter is dominated by a single peak near E_F, implying stronger hybridization in the latter. This can be attributed to the difference in the surface sensitivity of the two spectra due to the different kinetic energies of photoelectrons. This also indicates that the Ce valency at the surface is closer to trivalent than it is in the bulk.

In Fig. 2 we also show the XPS spectrum of the valence band taken with Mg $K\alpha$ radiation. Owing to the higher kinetic energies of photoelectrons, this spectrum is considered to be more bulk sensitive than the above PES spectra. Considering the photoionization cross sections,[26] the valence-band XPS spectrum should mainly reflect the Fe $3d$ partial density of states (DOS) with significant contributions from Ce $4f$ and Ce $5d$. As seen in the figure, the XPS spectrum shows a line shape similar to the off-resonance spectra of Ce $4d$-$4f$ and Ce $3d$-$4f$ resonant PES.

It is expected, that the BIS spectrum should also reflect the bulk electronic structure rather well. There is a peak near E_F and a broader feature at ~ 6 eV. They originate mainly from the Ce $4f$ states, although there are contributions from

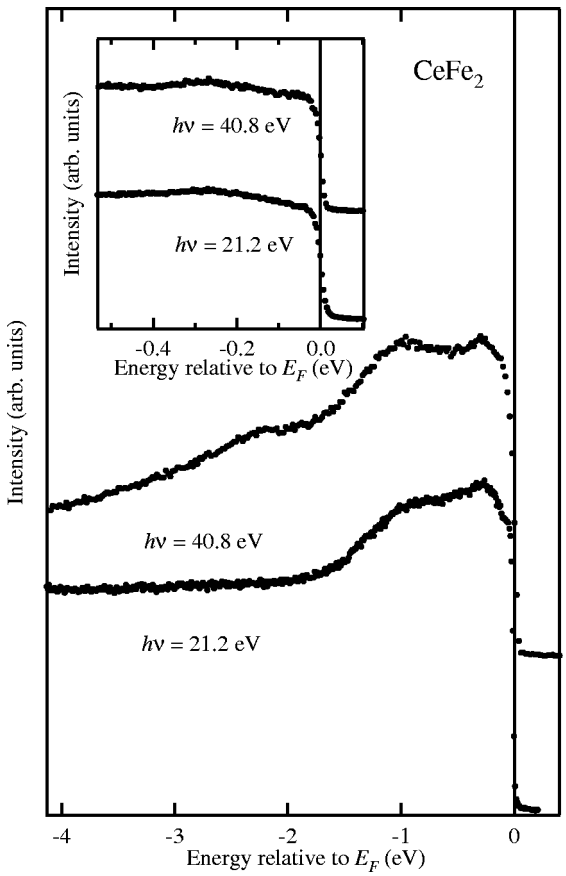

FIG. 3. High-resolution UPS spectra of $CeFe_2$. Inset shows an enlarged view near E_F.

the Ce $5d$ and Fe $3d$ states, too. The peak near E_F and the structure around ~ 6 eV correspond to the $4f^1$ and $4f^2$ final states, respectively.[2] The broad line shape of the structure at ~ 6 eV is due to the $4f^2$ final-state multiplet.[2] The strong intensity of the peak near E_F again indicates strong hybridization of the Ce $4f$ states with the valence states.

Figure 3 shows high-resolution UPS data. In this photon energy range, the cross sections of the Fe $3d$, Ce $4f$, and Ce $5d$ states varies rapidly with photon energy.[26] The relative cross section of Ce $4f$ to the other orbitals increases when going from $h\nu = 21.2$ to 40.8 eV while that of Ce $5d$ rapidly decreases. Therefore the structure at $-(2 \sim 3)$ eV which appears only in the $h\nu = 40.8$-eV spectrum, originates from the Ce $4f$ states, and corresponds to one of the double peaks in the Ce $4f$ spectrum obtained by the Ce $4d$-$4f$ resonant PES. This observation is also consistent with the fact that the 40.8 eV spectrum is surface sensitive, according to the ''universal curve'' of the mean free path of photoelectrons.[18] In the near E_F region, structures just below E_F and at ~ -0.3 eV are somewhat enhanced in the 40.8-eV spectrum. These structures originate from the Ce $4f$ states and correspond to the tail of the Kondo resonance (possibly with unresolved fine structures due to crystal-field splitting) and the spin-orbit side band, respectively. These structures are also expected to be dominated by surface contributions.

B. Single-impurity Anderson model

The SIAM parameters obtained in our calculation are listed in Table I. Here, ϵ_f is the position of the bare $4f$ level

TABLE I. SIAM parameters for $CeFe_2$. ϵ_f, U_{ff}, V, and U_{fc} are given in units of eV.

	ϵ_f	U_{ff}	V	U_{fc}	n_f
Surface	-1.8	6.4	0.23	9.7	1.0
Bulk	-0.8	6.4	0.41	9.7	0.78

($4f^1 \rightarrow 4f^0$ ionization level) relative to E_F, U_{ff} is the $4f$-$4f$ on-site Coulomb energy, U_{fc} is the $4f$-core-level Coulomb energy and V is the Ce $4f$-valence-band hybridization strength, in accordance with the definitions in Ref. 17. Using those parameters, the $4f$ occupation number n_f has been calculated and listed in the last column of Table I. Since we have fitted many different types of spectra using the SIAM shown in Fig. 4, many constraints have lead to a rather unique set of SIAM parameters.

In Fig. 4, comparison is made between the SIAM calculations and the experimental spectra. As seen, we obtain good overall agreement with all experimental spectra. The main discrepancy between the SIAM results and experimental spectra is found in the BIS spectrum [Fig. 4(c)], where the position of the calculated f^1 peak is about 0.5 eV lower than in the experimental spectrum. Noticeable from this figure is also the large difference between the bulk and surface spectra obtained through the SIAM analysis. For instance, in the Ce $4f$ spectrum obtained from Ce $4d$-$4f$ resonant PES [Fig. 4(b)], which is basically a double-peak structure, the relative strength of the two peaks is very different between the bulk spectrum and the surface spectrum. Similar differences in directly measured bulk- and surface spectra have previously been reported for Ce metal,[10] and can be explained as due to larger hybridization in the bulk.[15]

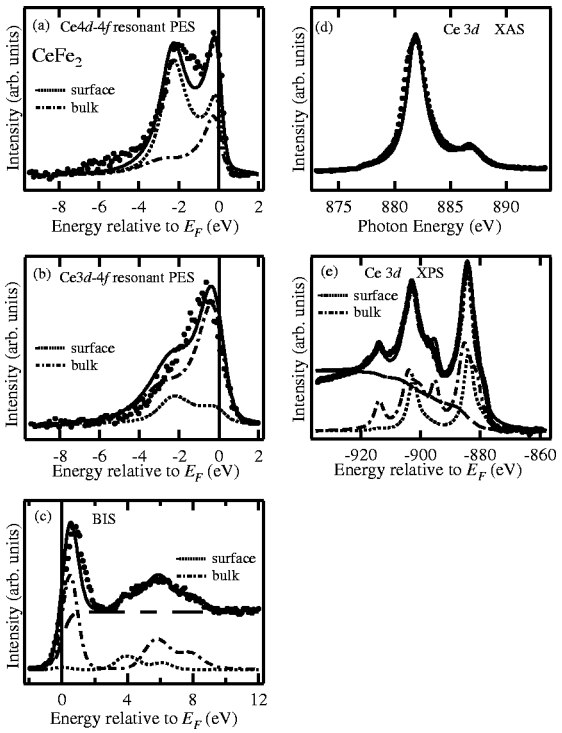

FIG. 4. Comparison of the single-impurity Anderson model calculation with the experimental spectra of $CeFe_2$. (a) Ce $4f$ spectrum obtained from Ce $4d$-$4f$ resonant PES. (b) Ce $4f$ spectrum obtained from Ce $3d$-$4f$ resonant PES. (c) BIS spectrum. (d) Ce $3d$ core-level XAS spectrum. (e) Ce $3d$ core-level XPS spectrum. In each panel, dots show experimental spectrum, solid curve shows the calculated spectrum, and dotted and dash-dotted curves show the calculated surface and bulk components, respectively.

Table I shows that, apparently, the Ce atoms belonging to the surface are as good as completely trivalent, with $n_f \simeq 1.0$, whereas in the bulk, the $4f$ states are strongly hybridized, having the significantly lower occupation of 0.78. However, there are noticeable amplitudes of the f^0 and f^2 configurations also at the surface, indicating that also here, some hybridization between the $4f$ and valence states is taking place.

C. Band-structure calculation

Experimentally, the partial moments in $CeFe_2$ have been studied using several different experimental methods: polarized neutrons,[27] Compton scattering[28] and, very recently, x-ray magnetic circular dichroism (XMCD).[29] In all experiments, an antiparallel coupling of the Ce and Fe moments is found. This coupling is also reproduced in our calculation, as well as in earlier calculations.[12,13] As is well known,[12] this antiparallel coupling of the moments is a strong indication that the Ce $4f$ states in $CeFe_2$ are delocalized. This can easily be understood from the following argumentation. If the $4f$ electrons are localized, the $4f$ spin moment would be dictated by the polarization of the spd electrons of the Ce atom, that via hybridization effects are known to be antiparallel to the $3d$ moment of the Fe atom. Hence the *spin* moments of the Ce atom and the Fe atom are always antiparallel, both in the localized and delocalized case. For localized $4f$ electrons, the $4f$ spin moment is accompanied by an orbital moment (larger than the spin moment) that (via Hund's third rule) is antiparallel to the Ce spin moment. Hence for localized $4f$ electrons the total (spin+orbital) Ce-Fe coupling is ferromagnetic, whereas if the Ce $4f$ orbital moment is quenched, due to band formation, the coupling is antiparallel.

In Fig. 5, the spin-resolved partial DOS for the Ce $4f$, Ce $5d$, and Fe $3d$ states are shown. The first and third panels show the majority spin channel for Ce and Fe, respectively, and the second and fourth panels show the minority spin channel. Comparing the DOS for Ce and Fe, we see that the Ce $4f$ and Fe $3d$ states have opposite spin polarization. Furthermore, the Ce $5d$ band width is seen to be much larger than that of the Ce $4f$ and Fe $3d$ states, with the magnitude of the Ce $5d$ DOS roughly an order of magnitude smaller than that of the Ce $4f$ and Fe $3d$ states.

Figure 6 shows the band structure of spin-polarized $CeFe_2$ along high-symmetry directions in the Brillouin zone. The flat bands clustered just above the Fermi level are predominantly of $4f$ character. In the region from ~ 2 to ~ 10 eV, and around -5 eV with respect to the Fermi level, the spin splitting of the bands is clearly visible.

Our calculated total spin magnetic moment amounts to $2.48\mu_B$ per formula unit (experimental saturation magnetization: $2.30\mu_B$, as stated earlier in this paper), with the main contributions being the Ce $4f$ moment $-0.54\mu_B$, the Ce $5d$ moment $-0.23\mu_B$, and the Fe $3d$ moment $1.75\mu_B$. The

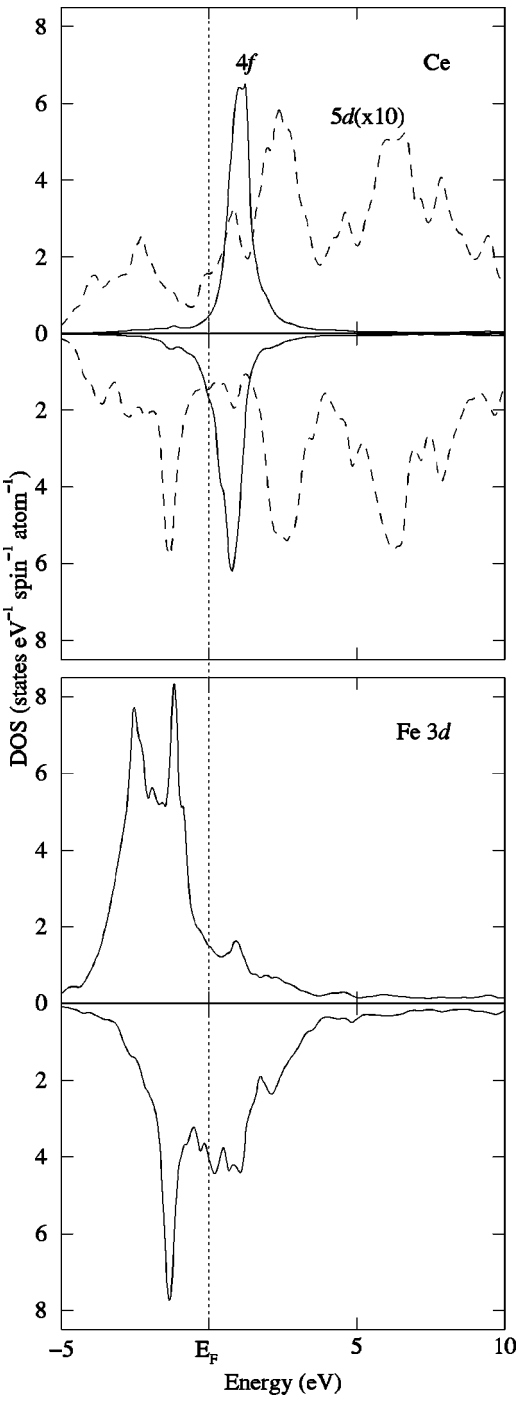

FIG. 5. Spin-resolved partial DOS for the Ce $4f$, Ce $5d$, and Fe $3d$ states. The Fermi energy is taken as the energy zero. The first and third panels show the majority spin channel, and the second and forth panels, the minority spin channel. In order to enhance visibility, the magnitude of the Ce $5d$ DOS (dashed line) has been multiplied by a factor of 10.

partial occupation numbers summed over spin, within the muffin-tin spheres, are 1.07 for Ce $4f$, 1.28 for Ce $5d$, and 6.18 for Fe $3d$. Note that the partial spin magnetic moments are calculated using the partial occupation numbers inside the muffin-tin spheres, which is somewhat arbitrary. The total spin moment is on the contrary, of course, well defined. An obvious point, which seems to have been overlooked so far, is that not only in band-structure calculations, but also

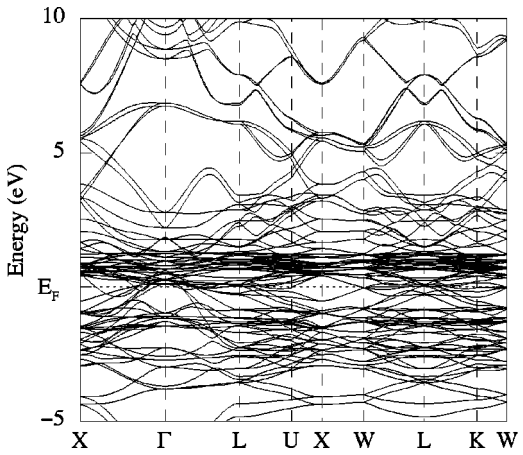

FIG. 6. Energy bands for $CeFe_2$ along high-symmetry directions. The Fermi energy is taken as the energy zero.

experimentally, the division of space between individual atomic species in a compound is in fact not unique nor even well defined. It is reasonable to believe that different experimental procedures differ in their ''volume of sensitivity'' around each atom, and thus effectively correspond to different ways of dividing up the total space in the compound between the atoms. This could be one reason why different experimental techniques find quite different values for the partial magnetic moments, and also why, in order to find the total Ce moment from experimental results, assumptions have to be made regarding the ratio of the number of $5d$ and $4f$ electrons contributing to the magnetization.[27] An analysis of experimental data along this direction of thought might help resolve controversies regarding the electronic structure of $CeFe_2$.[30]

A calculation of the moments including spin-orbit coupling and orbital polarization,[31] using the FP-LMTO method, has been performed earlier by Trygg *et al.*[13] The difference between the presently reported spin moments and the ones reported by Trygg *et al.*,[13] which include spin-orbit coupling, is very small, around 1%. Thus the effect of including spin-orbit coupling is shown to have only a very minor effect on the magnitude of the spin moment. Calculations by Eriksson *et al.*[12] using the atomic sphere approximation (ASA) give somewhat different values for the magnetic moments than the present method, in which no such geometrical approximation regarding the form of the potential, wave functions or charge density is made. As demonstrated in Ref. 13, the spin density in $CeFe_2$ is highly nonspherical, which may well be the reason for the differences in results from full-potential and ASA calculations. To summarize, the arguments presented above justify our present calculational approach, i.e., using a full-potential method, but neglecting spin-orbit coupling.

Concerning the absolute magnitudes of the individual moments, the discrepancies between different experimental approaches can be quite large, for instance, the Ce $4f$ spin moment is measured to be $-0.37\mu_B$ with XMCD, whereas polarized neutrons find the corresponding moment to be only about a fourth as large: $-0.10\mu_B$. As already touched upon above, one reason for these discrepancies between different experimental techniques may well be that they differ in the way the space in the compound is effectively divided up

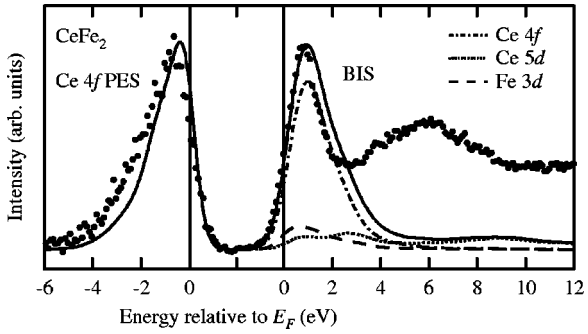

FIG. 7. Comparison of the DFT DOS with the experimental spectra. Dot-dashed curves show orbital components. In the PES part, the Ce $4f$ spectrum obtained by Ce $3d$-$4f$ resonant PES is shown.

between the atoms. With this in mind, the magnitudes of our calculated moments must be said to be in satisfactory agreement with experimental findings, although the overall trend appears to be that the calculations overestimate the moment magnitudes.

In Fig. 7, we compare the valence-band Ce $4f$ PES and BIS spectra with the DFT DOS. As mentioned earlier, the Ce $3d$-$4f$ resonant PES spectrum and the BIS spectrum are rather bulk sensitive, and thus it is relevant to compare these spectra with bulk DFT calculations. In the PES part of the spectra, comparison is made between the experimentally obtained Ce $4f$ spectra and the Ce $4f$-projected DFT DOS. As for the BIS part, the Ce $4f$, $5d$, and Fe $3d$ partial DOS have been added taking account of the atomic photoionization cross sections.[26] Agreement between experiment and theory is satisfactory almost to the same extent as in the SIAM calculation. In the DFT DOS, the structure around 6 eV in the BIS spectrum is of course not reproduced, since this structure corresponds to the $4f^2$ final state, and thus is a purely excited-state property of the system. Furthermore, in the DFT calculation, the energy of the near E_F peak in the Ce $4f$ PES spectrum and also in the BIS spectrum is slightly higher than in the experimental spectra. Also, the intensity on the higher binding energy side of the PES spectrum is underestimated in the calculation. However, one should note that the relative intensities depend also on the transition matrix elements, which are not included in the DOS curves.

Figure 8 shows the valence-band XPS, Ce $3d$-$4f$, and $4d$-$4f$ off-resonance and UPS (He II) spectra. The spectral weight comes primarily from the Fe $3d$ states, and thus we compare these spectra with the Fe $3d$ partial DFT DOS. Although there are differences in the surface sensitivity and in the contributions from other orbitals, all the experimental spectra have similar band widths and line shapes. In comparison with the DFT DOS, although overall features are well reproduced, the experimental spectra have larger spectral weight near E_F than the calculated DOS.

IV. DISCUSSION AND CONCLUSIONS

Generally, for any material, the surface electronic structure can differ substantially from the bulk one. For valence fluctuating systems like $CeFe_2$, it is very likely that the electronic structure of the Ce atoms close to the surface is not the same as that of the bulk Ce atoms. Therefore, in order to

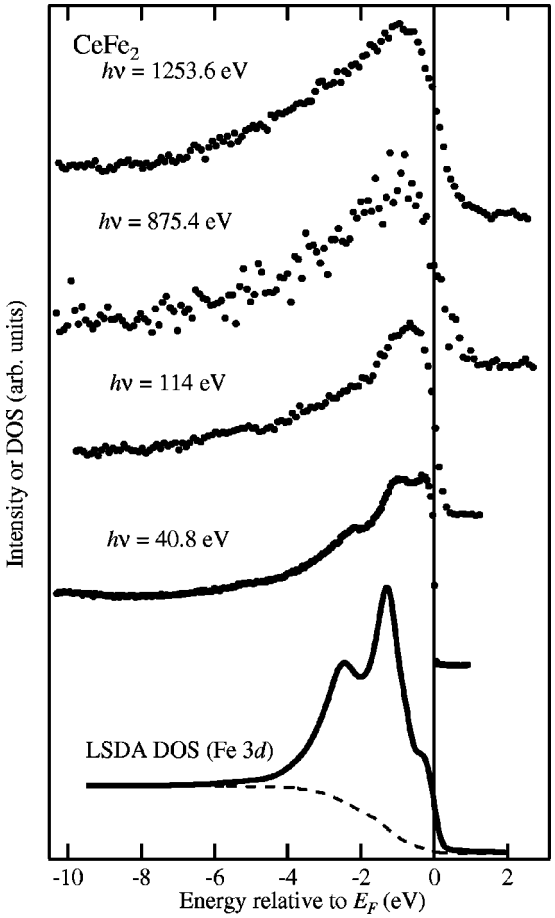

FIG. 8. Valence-band PES spectra of $CeFe_2$ taken at various photon energies compared with the Fe $3d$ partial density of states from the band-structure calculation. The DFT DOS has been broadened with the experimental resolution of the 114-eV spectrum.

study the bulk electronic structure of valence fluctuating Ce compounds by means of high-energy spectroscopic methods, it is essential to take into account the effects of the sample surface when interpreting the spectra. In the present work, by assuming that the spectra are superpositions of the surface and bulk components, we have shown that all measured spectra of $CeFe_2$ are fairly well reproduced by the SIAM calculations using the same set of parameters. At the surface, Ce is found to be nearly trivalent. The bulk set of parameters places $CeFe_2$ in the strongly intermediate-valent regime, giving a $4f$-occupation number n_f as small as 0.78 (with considerable amplitude of the f^2 configuration both in the surface and bulk). This means that the Ce $4f$ states are strongly hybridized with the Fe $3d$ states in the bulk and that the states around E_F have a large amount of f character. Also, the differences between our SIAM-derived bulk- and surface spectra for $CeFe_2$ are similar to the differences between directly measured bulk- and surface spectra of Ce metal, a difference which can be explained as due to larger $4f$ hybridization in the bulk than at the surface.

Apart from the SIAM analysis, a number of features of the measured spectra force us to draw the same conclusion regarding the nature of the $4f$ states in the bulk and at the surface, notably the large difference between the Ce $4f$ spectra obtained from the Ce $3d$-$4f$ and Ce $4d$-$4f$ resonant PES,

and the strong intensity of the peak near E_F in the BIS spectrum.

As a result of the strong hybridization of the Ce $4f$ states in the bulk, the ''f^0'' final state feature in the Ce $4f$ spectrum deduced from the Ce $3d$-$4f$ resonant PES has a very weak intensity in contrast to the Ce $4d$-$4f$ resonant PES spectrum, where the f^0-final-state feature leads to the well-known double-peak structure. In such a case, i.e., where there is strong screening of excitations, it is expected that the bulk $4f$ spectrum can be interpreted in terms of a one-electron picture, and thus the DFT DOS should compare well with the $4f$ spectrum. This is also seen to be the case. Comparison of the $4f$ spectra with the DOS (Fig. 7) shows that the Ce $4f$ partial DFT DOS describes the valence-band Ce $4f$ spectra well, except for the f^2 structure in the BIS spectrum of course, since the f^2 peak is due to incomplete screening. This fact poses the question of how the ''f^1'' final state (which is commonly referred to as the ''Kondo peak'') of the SIAM picture and ''the $4f$ band'' in the band picture are related to each other, since according to DFT, this peak is a one-electron feature, and in the SIAM, this is due to a many-body effect.

We also draw the conclusion that due to the strong hybridization in the bulk, the spin-orbit side band seen in the high-resolution UPS spectra (Fig. 3) must have surface origin since it is known that the spectral weight of the spin-orbit side band is strongly reduced when the hybridization is strong.[10]

We now turn to a more detailed comparison of how well the DFT calculations and the SIAM analysis perform for the different spectra. Regarding the position of the near E_F peak in the BIS spectrum, the DFT calculation predicts a higher energy than experiment while the SIAM calculation predicts a lower energy than experiment. The intensity on the higher binding energy side of the near E_F peak in the PES spectrum is underestimated in the DFT calculation (although strictly speaking, intensities cannot be expected to be reproduced with a DOS, since the transition matrix elements are neglected) while it is overestimated in the SIAM calculation. The position of the near E_F peak in the PES spectra is calculated to be too close to E_F both in the SIAM and DFT calculations. As for the Fe $3d$ component, the DOS calculated using DFT does not give a good account of the intensity in the experimental spectra near E_F. This may be due to that the $4f$ transition matrix elements are large close to the Fermi level compared to the $3d$ transition matrix elements.

All in all, the above discussion amounts to that the Ce $4f$ electrons in the bulk hybridize strongly with the Fe $3d$ electrons. This conclusion agrees perfectly with the experimentally observed antiparallel coupling of the Ce and Fe moments, which is also reproduced in the DFT calculation. In the SIAM, the $4f$ electron is assumed to be localized, which indirectly implies that a parallel coupling of the Ce and Fe moments is expected.

Finally, we wish to mention some sources of error in the present work. Our measurements were done on scraped surfaces, which might make the surface rough, and therefore ill defined. Furthermore, the precise values of photoelectron mean free paths are difficult to estimate, which naturally also has the effect of making the border between ''bulk'' and ''surface'' somewhat ill defined. Our SIAM is not the most elaborate one, for instance we assume a degeneracy of 14 of the $4f$ level, thereby neglecting spin-orbit coupling and anisotropic hybridization effects, which leads to a crystal-field splitting. Furthermore, as in all DFT calculations, the functional used treats electron correlation only to a limited extent, i.e., it is not meaningful to expect perfect agreement between the DFT results and experiment.

ACKNOWLEDGMENTS

The authors thank the staff of SOR-RING, Y. Azuma, T. Miyahara, and the staff of Photon Factory for technical support. The authors also thank A. Sekiyama, J. Okamoto, T. Tsujioka, and T. Saitoh for help in the experiment. A.D. acknowledges financial support from the Swedish Foundation for International Cooperation in Research and Higher Education. Part of this work has been done under the approval of the Photon Factory Program Advisory Committee (Proposal No. 94G361). A.D. and O.E. are grateful to J. M. Wills for supplying the full potential code used in this study.

*Present address: Department of Chemistry, Chiba University, Chiba 263-8522, Japan.

[1] A. Amato, Rev. Mod. Phys. **69**, 1119 (1997).

[2] J.W. Allen, S.J. Oh, O. Gunnarsson, K. Schönhammer, M.B. Maple, M.S. Torikachvili, and I. Lindau, Adv. Phys. **35**, 275 (1986).

[3] E. Weschke, C. Laubschat, R. Ecker, A. Höhr, M. Domke, G. Kaindl, L. Severin, and B. Johansson, Phys. Rev. Lett. **69**, 1792 (1992).

[4] J. Déportes, D. Givord, and K.R.A. Ziebeck, J. Appl. Phys. **52**, 2074 (1981).

[5] K.H.J. Buschow, Rep. Prog. Phys. **40**, 1179 (1977).

[6] Y. Nishihara, J. Magn. Magn. Mater. **70**, 75 (1987).

[7] L. Paolasini, P. Dervenagas, P. Vulliet, J.-P. Sanches, G.H. Lander, A. Hiess, A. Panchula, and P. Canfield, Phys. Rev. B **58**, 12117 (1998).

[8] M. Croft, R. Neifeld, B. Qi, G. Liang, I. Perez, S. Gunapala, F. Lu, S. A. Shaheen, E. G. Spencer, N. Stoffel, and M. den Boer, in *Proceedings of the Fifth International Conference on Valence Fluctuations (Bangalore)* 1986, edited by S. K. Malik and L. C. Gupta (Plenum, New York, 1987), p. 217.

[9] C. Laubschat, E. Weschke, C. Holtz, M. Domke, O. Strebel, and G. Kaindl, Phys. Rev. Lett. **65**, 1639 (1990).

[10] E. Weschke, C. Laubschat, T. Simmons, M. Domke, O. Strebel, and G. Kaindl, Phys. Rev. B **44**, 8304 (1991).

[11] C. Laubschat, E. Weschke, M. Domke, T. Simmons, and G. Kaindl, Surf. Sci. **269/270**, 605 (1992).

[12] O. Eriksson, L. Nordström, M.S.S. Brooks, and B. Johansson, Phys. Rev. Lett. **60**, 2523 (1988).

[13] J. Trygg, J.M. Wills, B. Johansson, and O. Eriksson, Phys. Rev. B **50**, 4200 (1994).

[14] A. Sekiyama, T. Iwasaki, K. Matsuda, Y. Saitoh, Y. Onuki, and S. Suga, Nature (London) **403**, 396 (2000).

[15] O. Gunnarsson and K. Schönhammer, Phys. Rev. Lett. **50**, 604 (1983); Phys. Rev. B **28**, 4315 (1983); *ibid.* **31**, 4815 (1985).

[16] O. Gunnarsson and O. Jepsen, Phys. Rev. B **38**, 3568 (1988).

[17] A. Kotani, T. Jo, and J.C. Parlebas, Adv. Phys. **37**, 37 (1988).

[18] D. A. Shirley, in *Photoemission in Solids I*, edited by M. Cardona

and L. Ley (Springer-Verlag, Berlin, 1978), p. 165.
[19] J. M. Wills (unpublished); J.M. Wills and B.R. Cooper, Phys. Rev. B **36**, 3809 (1987); D.L. Price and B.R. Cooper, *ibid.* **39**, 4945 (1989).
[20] P. Hohenberg and W. Kohn, Phys. Rev. **136**, B864 (1964); W. Kohn and L.J. Sham, Phys. Rev. **140**, A1133 (1965).
[21] L. Hedin and B.I. Lundqvist, J. Phys. C **4**, 2064 (1971).
[22] O.K. Andersen, Phys. Rev. B **12**, 3060 (1975); H. L. Skriver, *The LMTO Method* (Springer, Berlin, 1984).
[23] D.J. Chadi and M.L. Cohen, Phys. Rev. B **8**, 5747 (1973); S. Froyen, Phys. Rev. B **39**, 3168 (1989).
[24] Y. Baer, R. Hauger, C. Zurcher, M. Campagnea, and G.K. Wertheim, Phys. Rev. B **18**, 4433 (1978).
[25] J.C. Fuggle, M. Campagna, Z. Zolnierik, and R. Lässer, Phys. Rev. Lett. **45**, 1597 (1980).
[26] J.J. Yeh and I. Lindau, At. Data Nucl. Data Tables **32**, 1 (1985).
[27] S.J. Kennedy, P.J. Brown, and B.R. Coles, J. Phys.: Condens. Matter **5**, 5169 (1993).
[28] M.J. Cooper, P.K. Lawson, M.A.G. Dixon, E. Zukowski, D.N. Timms, F. Itoh, H. Sakurai, H. Kawata, Y. Tanaka, and M. Ito, Phys. Rev. B **54**, 4068 (1996).
[29] A. Delobbe, A.M. Dias, M. Finazzi, L. Stichauer, J.P. Kappler, and G. Krill, Europhys. Lett. **43**, 320 (1998).
[30] A.P. Murani and P.J. Brown, Europhys. Lett. **48**, 353 (1999); A. Delobbe, A.M. Dias, M. Finazzi, L. Stichauer, J.P. Kappler, and G. Krill, *ibid.* **48**, 355 (1999);
[31] O. Eriksson, M.S.S. Brooks, and B. Johansson, Phys. Rev. B **41**, 7311 (1990).